Dalton Transactions

Synthesis, characterization, and polymerization of capped paddlewheel porous cages

Journal:	*Dalton Transactions*
Manuscript ID	DT-COM-12-2020-004361.R1
Article Type:	Communication
Date Submitted by the Author:	27-Jan-2021
Complete List of Authors:	Deegan, Meaghan; University of Delaware, Chemistry and Biochemistry Bloch, Eric; University of Delaware, Chemistry and Biochemistry

COMMUNICATION

Synthesis, characterization, and polymerization of capped paddlewheel porous cages

Meaghan M. Deegan[a] and Eric D. Bloch*[a,b]

Received 00th January 20xx,
Accepted 00th January 20xx

DOI: 10.1039/x0xx00000x

Although paddlewheel-based structures are common among permanently porous metal-organic materials, suitable strategies for the isolation of metal node-terminated, capped paddlewheel-based cage structures remain limited. We explored the use of chelating dicarboxylate ligand derivates (esp) for the isolation of trimesate-linked cages, $Mo_{12}(btc)_4(esp)_6$, that are structural analogs of the small octahedral pore of HKUST-1. The porosity of these novel cages is appreciably higher than previously reported structures of this type. We also demonstrate that pillaring the isolated cage with DABCO generated an amorphous polymer that featured exceptional thermal stability and enhanced porosity.

Studies of highly porous metal-organic materials have largely emphasized two and three-dimensional frameworks (MOFs),[1] but work over the past several years has significantly expanded upon reports of molecular, permanently porous coordination cages (PCCs).[2] Recent work has demonstrated that cages can be isolated as highly porous solids, with a record BET surface area in excess of 1300 m^2/g reported last year.[3] PCCs have many of the properties of MOFs that make them highly attractive for diverse applications,[4,5,6] while their molecular nature and resultant solubility can offer advantages for material purification and processing.[7] A close structural relationship exists between many common coordination cages and MOF pores.[8] For instance, a family of Cp-capped Zr cages has been described that are close structural analogs of the tetrahedral pore in the UiO series of frameworks.[9,10,11] A number of octahedral calixarene-capped cages have been described[12,13,14] that feature tetrahedral node structures linked by tritopic bridging carboxylate ligands that closely mimic the octahedral pores found in the PCN-9[15] and M-BTT[16,17] families of frameworks.

Materials featuring bimetallic paddlewheel nodes are common for MOFs and represent a large subset of all reported PCCs.[18] Among these molecular materials, the most extensively studied structures are cuboctahedral cages, $M_{24}(1,3\text{-bdc})_{24}$, which have been reported for a number of different transition metals and isophthalic acid derivatives.[3,19,20,21] Analogous pore structures are incorporated in a number of MOFs including HKUST-1.[22–25] Isolation of molecular analogs of node-terminated structures, including the small and medium HKUST-1 pores, requires the application of a suitable capping strategy. The development of approaches to isolate molecular analogs of the small HKUST-1 pore, in particular, remains an attractive target, as gas is preferentially stored in these sites.[26] In this area, early work from Cotton and co-workers demonstrated that structural analogs of the small, octahedral HKUST-1 pore could be accessed by capping Mo_2 and Rh_2 paddlewheels with formamidine ligands.[27,28] More recently, our group built upon their approach to access molecular analogs of both the small and medium HKUST-1 pores that incorporate Mo_2 and Cu_2 nodes (Figure 1).[29] Further, it was shown for the first time that cages of this type could be isolated as permanently porous solids, with BET surface areas as high as 446 m^2/g. Given the limited work exploring the synthesis and porosity of capped paddlewheel cages, we set out to explore an alternative cage capping strategy to access highly porous structural analogs of the small HKUST-1 pore.

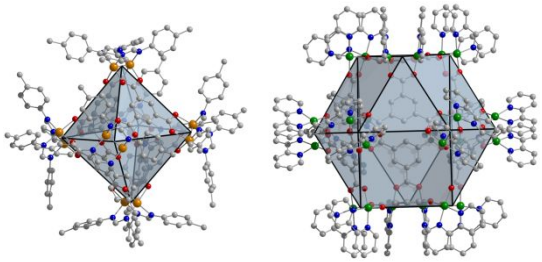

Fig. 1 Previously reported structures of octahedral (left) and cuboctahedral (right) capped-paddlewheel porous coordination cages.

To direct the *cis*-coordination of a paddlewheel capping ligand, we targeted the use of a chelating dicarboxylate capable of selectively bridging adjacent sites of a paddlewheel. One platform that was developed to support this coordination mode is bis(tetramethyl-1,3-benzenedipropionate) (H-esp, Figure

[a] *Department of Chemistry & Biochemistry, University of Delaware, Newark, Delaware 19716, USA. E-mail: edb@udel.edu*
Electronic Supplementary Information (ESI) available: experimental details, spectroscopic data, gas adsorption data. See DOI: 10.1039/x0xx00000x

2).[30–35] This ligand platform has the advantage in that it is readily compatible with arene functionalization, where appended residues can play a critical role in controlling cage formation, solid-state packing, crystallinity, stability, and porosity.[36,37]

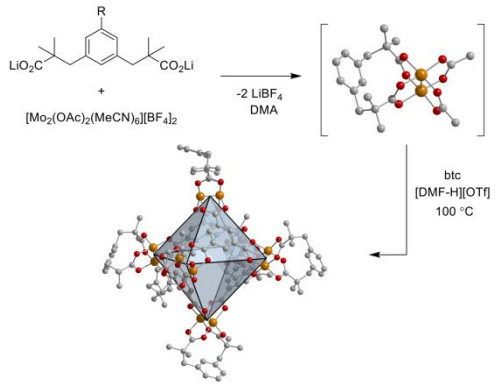

Fig. 2 Synthesis of octahedral esp-supported paddlewheel cages.

We explored the reactivity of the previously reported unfunctionalized ligand (H-esp) and a novel 5-^{t}Bu-functionalized derivative (^{t}Bu-esp) that could be accessed via a similar synthetic protocol (Figure 2). Reaction conditions that were initially explored for cage generation by combining the esp ligand with trimesic acid and a variety of divalent metal salts typically yielded product mixtures with poor selectivity for molecular capped cage phases. Selective formation of the desired cage phase was instead achieved by starting from a more reactive, asymmetric molybdenum precursor, $[Mo_2(OAc)_2(MeCN)_6][BF_4]_2$ (Figure 2). *In situ* combination of this precursor with the deprotonated ligand, H-espLi_2, in DMA led to the rapid generation of the asymmetric esp-ligated paddlewheel, Mo_2(H-esp)$(OAc)_2$(solv)$_x$, as indicated by a rapid color change from pink-orange to yellow. Subsequent addition of trimesic acid (btc) followed by heating at 100 °C overnight in the presence of acid (dimethylformamidium triflate; [DMF-H][OTf]) yielded a homogenous red solution. The cage product was precipitated from this mixture as an amorphous red-orange solid upon the addition of excess methanol. Application of a directly analogous synthetic approach provided access to an isolated cage that instead incorporated the ^{t}Bu-esp ligand.

Despite extensive efforts, these cage materials have not been isolable as highly crystalline phases. This is perhaps explained by considering the symmetry and flexibility of the supporting ligand at the capped paddlewheel unit. Previous approaches that allowed for the isolation of highly crystalline cage phases employed rigid formamidine or bipyridine ligands that have symmetry planes both parallel and perpendicular to the metal-metal axis in the capped paddlewheel unit. In contrast, the esp ligand is more flexible, with the ligand preferentially adopting a conformation that lacks a symmetry plane perpendicular to the metal-metal axis in reported paddlewheel structures.[31,32,33,34,35] This may disrupt the three-dimensional packing of these materials and preclude the formation of highly-ordered crystalline phases. An additional factor that may contribute to the poor crystallinity of the generated materials is the possibility that cages are generated as a mixture of both a small octahedral cage, $Mo_{12}(btc)_4(esp)_6$, and a medium cuboctahedral cage, $Mo_{24}(btc)_8(esp)_{12}$.

Given the challenges associated with obtaining solid-state structural information to assess the identity of the isolated cage phases, we instead turned to alternative characterization methods. The previously reported Mo_2 capped paddlewheel cage, $Mo_{12}(btc)_4(DTolF)_{12}$ served as a useful handle for the spectroscopic signature of the Mo_2 paddlewheel unit and for assessing the size of the small octahedral cage.[29] The UV-visible spectra of the isolated esp and ^{t}Bu-esp capped cages in pyridine have an absorption feature associated with the Mo_2-paddlewheel unit centered around 425 nm, nearly identical to that observed for $Mo_{12}(btc)_4(DTolF)_{12}$ (Figure S5.1). This is appreciably shifted from the bright yellow, symmetric $(esp)_2Mo_2$ complex, whose peak absorption is centered around 275 nm in pyridine, consistent with coordination of the bridging trimesate ligand in the cages. The carbonyl stretch associated with the molybdenum-bound esp or ^{t}Bu-esp ligand is readily identified at 1515 cm^{-1} in the cage IR spectra, which is shifted slightly from the symmetric $(esp)_2Mo_2$ complex (ν_{CO} = 1505 cm^{-1}) (Figures S3.1-S3.4) The trimesic acid carbonyl stretch well-resolved just above 1600 cm^{-1} for both cages, with additional carbonyl stretches associated with amide solvent apparent in the cage spectra between 1650 and 1700 cm^{-1}.

Solution phase NMR spectra of both the esp and ^{t}Bu-esp capped cages have very broad resonances that show incorporation of both the capping carboxylate ligands and the trimesate bridge (Figures S2.7-S2.8). The observed spectra are consistent with cage formation, although their integrations cannot distinguish between the small and medium capped cage isomers. We turned to DOSY experiments to measure the rate of diffusion of the cages in order to estimate their sizes (Figures S2.10-S2.12). As a starting point, we carried out the same experiment for the octahedral $Mo_{12}(btc)_4(DTolF)_{12}$ cage, with measured diffusion rates ranging from 3.2 to 3.5 x 10^{-10} m^2/s in pyridine solution. The size of the cage approximated as sphere was estimated by application of the Stokes-Einstein equation, with a calculated radius of 7.1-7.75 Å. For the esp-capped cages, the broadness of the NMR spectra complicated their characterization using the DOSY method and gave rise to very broad cross peaks and measured diffusion rates that vary widely. The experimentally determined rates were used to estimate cage radii that vary from 8-15 Å for the esp-capped cage and 10-19 Å for the ^{t}Bu-functionalized derivative. These values do not reliably discriminate between the two proposed structures.[10] To more carefully assess this possibility, we compared the pore size distributions for the H-esp and ^{t}Bu-esp capped cages to previously reported capped paddlewheel cages. This analysis is more consistent with the esp-capped cages existing predominantly as the small octahedral structure.

The precipitated amorphous esp-capped cage was non-porous to N_2, with a modest CO_2 accessible BET (Langmuir) surface area of 218 (356) m^2/g. For molecular materials, the ability to control cage packing can be crucial for manipulating material porosity, where slight changes to synthetic conditions, solvent exchange protocols, and activation methods can give

rise to phases with vastly different surface areas.[38] We found that dissolution of the precipitated cage in either THF or pyridine followed by solvent removal *in vacuo* generated a dense red film. Following MeOH washes, this approach yielded a much higher surface area material, with N_2 accessible Langmuir surface areas between 800-1000 m^2/g. Material prepared via initial evaporation of a pyridine solution was found to have an N_2 accessible BET (Langmuir) surface area of 770 (866) m^2/g and a CO_2 accessible BET (Langmuir) surface area of 616 (909) m^2/g (Figure 3). Similar overall behavior was observed for the ^{t}Bu-esp cage derivative, albeit with the optimally activated cage phase exhibiting slightly lower porosity. Here, N_2 and CO_2 accessible BET (Langmuir) surface areas were determined to be 696 (785) m^2/g and 529 (902) m^2/g, respectively. We note here that the surface areas accessible for either of these novel cages are appreciably higher than those reported using alternative paddlewheel capping strategies.[29]

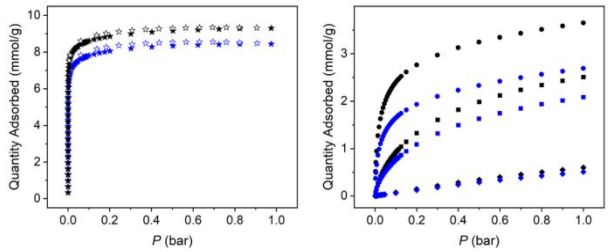

Fig. 3 Gas adsorption in $Mo_{12}(btc)_4(H\text{-}esp)_6$ (black) and $Mo_{12}(btc)_4(^t Bu\text{-}esp)_6$ (blue) Left: N_2 adsorption (closed stars) and desorption (open stars) measured at 77 K. Right: Room temperature hydrocarbon adsorption with circles, squares and diamonds representing propane, ethane and methane, respectively.

The high surface areas of the synthesized cages relative to previously reported capped paddlewheel structures of this type prompted us to explore their behavior toward hydrocarbon adsorption. Notable for structurally related systems, the small, octahedral cage structure in HKUST-1 is well known to serve as a preferential methane binding site.[26] The high methane uptake in the related octahedral structure of the well-studied organic cage CC3-R, was both rationalized in analogy to the HKUST-1 pore and motivated our interest in examining the adsorption of hydrocarbons in our structurally related PCCs.[39] First, we compared the low pressure, 298 K adsorption of methane, ethane, and propane in the H-esp and ^{t}Bu-esp capped cages. While the two cages uptake similar amounts of methane (0.60 vs. 0.51 mmol/g at 1 bar), an appreciably lower propane uptake is observed in the *tert*-butyl functionalized material (3.65 vs. 2.69 mmol/g at 1 bar). This is consistent with functionalization of the capping ligand with a bulky *tert*-butyl group blocking otherwise accessible void space and lowering the uptake of larger guests such as propane. This is consisted with the incorporated functional groups blocking larger guests from entering void space that is accessible for the unfunctionalized derivative. Examination of the high-pressure methane adsorption in the esp-capped cage revealed a total methane uptake of 90 cm^3/g at 65 bar. The relatively high methane uptake for this material given its only moderate surface area is consistent with the preferential adsorption of methane in the small octahedral pore structure. Further, the ability to access this uptake when the material is processed in a dense, amorphous state is a promising preliminary result toward the development of dense materials with high, bulk volumetric gas uptakes. The ability to easily generate a dense porous phase from these molecular materials offers a significant advantage over typical three-dimensional porous solids, which are typically synthesized as low-density solids that are not readily manipulated to generate more dense bulk materials.[40]

One limitation of these and many other molecular cage-based porous materials is a lack of strong inter-cage interactions to enforce their three-dimensional packing upon desolvation. For the above cages, a decrease in surface area is observed upon activation above room temperature. One approach to control cage packing and enhance their stability toward solvent removal is to generate polymeric cage phases either through the addition of pillaring ligands or via ligand cross-linking.[41,42,43] For each paddlewheel, two coordination sites are potentially available to bind exogenous pillaring ligands, with twelve sites total per cage. All of these sites are oriented toward the four open faces of the octahedral cage structure, with three sites available for ligand binding at each of these faces. The addition of DABCO (4 equiv) to a homogenous solution of cage led to the precipitation of an amorphous solid upon heating (Figure 4). We hypothesize that the disordered structure of this material is partially attributable to random pillaring at a maximum of one site per open cage face due to steric constraints. Further, the ability to access polymerized cage-based materials provides additional, circumstantial evidence that favors the octahedral cage structure over the cuboctahedral cage, as the directional orientation of the open metal sites in the larger structure would likely preclude polymerization with a short, structurally rigid bridging ligand such as DABCO.

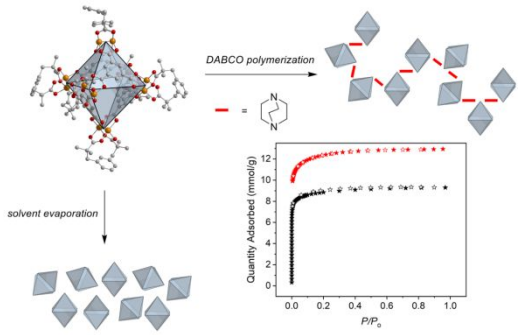

Fig. 4 Two-dimensional representation of control over solid-state packing through polymerization in the presence of DABCO (top) in comparison to isolation as an amorphous film (left). Enhanced porosity is observed in the DABCO polymer (bottom right), with 77 K N_2 adsorption (closed stars) and desorption (open stars) shown for the DABCO polymer (red) and the molecular cage, $Mo_{12}(btc)_4(esp)_6$ (black).

Examination of the stability and porosity of the cage-based polymer revealed behavior distinct from the isolated molecular cages. An activation temperature survey revealed that the porosity of the material increased with temperature to a Langmuir surface area of roughly 1100 m^2/g following activation at 200 °C, with similar porosity maintained up to temperatures as high as 350 °C. Upon activation, sublimation of some incorporated DABCO was observed, thus, to obtain an optimally activated material free of excess DABCO, a second THF wash

was carried out to remove free DABCO after initial activation followed by reactivation at 200 °C. Under these conditions, a material with a BET (Langmuir) surface area of 1072 (1207) m^2/g was obtained (Figure 4). The DABCO-pillared cage polymer also displayed higher porosity toward CH_4, with a total methane uptake of 124 cm^3/g at 195 K and 1.2 bar as compared with an uptake of 91 cm^3/g for the molecular cage.

This study outlined an alternative approach to the generation of capped paddlewheel-based coordination cages that provided access to cages with higher accessible surface areas than previously reported structures of this type. The stability and porosity these structures could be enhanced further by incorporating the synthesized cages in an amorphous, DABCO-pillared polymer. Preliminary studies of hydrocarbon adsorption in these materials revealed relatively high methane capacities for the amorphous cages and motivates our ongoing interest in developing these and related structures as dense materials for gas storage applications. Ongoing efforts in our lab are interested in expanding upon this ligand capping strategy to access structures of this type with other metals. Further, we hope to build upon this polymerization strategy to access higher surface area materials from porous molecular cages.

This material is based upon work supported by the U.S. Department of Energy's Office of Energy Efficiency and Renewable Energy under the Hydrogen and Fuel Cell Technologies and Vehicle Technologies Offices under Award Number DE-EE0008813. We thank Alexandra Antonio for help with SEM experiments.

Conflicts of interest

There are no conflicts to declare.

References

1 H. Furukawa, K. E. Cordova, M. O'Keeffe and O. M. Yaghi, *Science*, 2013, **341**, 1230444.
2 A. J. Gosselin, C. A. Rowland and E. D. Bloch, *Chem. Rev.*, 2020, **120**, 8987-9014.
3 G. R. Lorzing, A. J. Gosselin, B. A. Trump, A. H. P. York, A. Sturluson, C. A. Rowland, G. P. A. Yap, C. M. Brown, C. M. Simon and E. D. Bloch, *J. Am. Chem. Soc.*, 2019, **141**, 12128-12138.
4 N. Ahmad, H. A. Younus, A. H. Chughtai and F. Verpoort, *Chem. Soc. Rev.*, 2015, **44**, 9-25.
5 T. S. Koblenz, J. Wassenaar and J. N. H. Reek, *Chem. Soc. Rev.*, 2008, **37**, 247-262.
6 M. M. Deegan, M. R. Dworzak, A. J. Gosselin, K. J. Korman and E. D. Bloch, *Chem. Eur. J.*, 2021, Accepted. (doi: 10.1002/chem.202003864).
7 S. Mollick, S. Fajal, S. Mukherjee and S. K. Ghosh, *Chem. Asian J.*, 2019, **14**, 3096-3108.
8 G. E. Decker, G. R. Lorzing, M. M. Deegan and E. D. Bloch, *J. Mater. Chem. A*, 2020, **8**, 4217-4229.
9 G. Liu, Z. Ju, D. Yuan and M. Hong, *Inorg. Chem.*, 2013, 52, 13815-13817.
10 A. J. Gosselin, G. E. Decker, B. W. McNichols, J. E. Baumann, G. P. A. Yap, A. Sellinger and E. D. Bloch, *Chem. Mater.*, 2020, **32**, 5872-5878.
11 J. H. Cavka, S. Jakobsen, U. Olsbye, N. Guillou, C. Lamberti, S. Bordiga and K. P. Lillerud, *J. Am Chem. Soc.*, 2008, **130**, 13850-13851.
12 F.-R. Dai and Z. Wang, *J. Am. Chem. Soc.*, 2012, **134**, 8002-8005.
13 M. Liu, W. Liao, C. Hu, S. Du and H. Zhang, *Angew. Chem. Int. Ed.*, 2012, **51**, 1585-1588.
14 M. M. Deegan, T. S. Ahmed, G. P. A. Yap, and E. D. Bloch, *Chem. Sci.*, 2020, **11**, 5273-5279.
15 S. Ma and H.-C. Zhou, *J. Am. Chem. Soc.*, 2006, **128**, 11734-11735.
16 M. Dincă, A. Dailly, Y. Liu, C. M. Brown, D. A. Neumann and J. R. Long, *J. Am. Chem. Soc.*, 2006, **128**, 16876-16883.
17 E. D. Bloch, W. L. Queen, M. R. Hudson, J. A. Mason, D. J. Xiao, L. J. Murray, R. Flacau, C. M. Brown and J. R. Long, *Angew. Chem. Int. Ed.*, 2016, **55**, 8605-8609.
18 M. Köberl, M. Cokoja, W. A. Herrmann and F. E. Kühn, *Dalton Trans.*, 2011, **40**, 6834-6859.
19 M. Eddaoudi, J. Kin, J. B. Wachter, H. K. Chae, M. O'Keeffe and O. M. Yaghi, *J. Am. Chem. Soc.*, 2001, **123**, 4368-4369.
20 B. Moulton, J. Lu, A. Mondal and M. J. Zaworotko, *Chem. Commun.*, 2001, 863-864.
21 Y. Ke, D. J. Collins and H.-C. Zhou, *Inorg. Chem.*, 2005, **44**, 4154-4156.
22 S. S.-Y. Chui, S. M.-F. Lo, J. P. H. Charmant, A. G. Orpen and I. D. A. Williams, *Science*, 1999, **283**, 1148-1150.
23 M. Kramer, S. B. Ulrich and S. Kaskel, *J. Mater. Chem.*, 2006, **16**, 2245-2248.
24 L. J. Murray, M. Dinca, J. Yano, S. Chavan, S. Bordiga, C. M. Brown and J. R. Long, *J. Am. Chem. Soc.*, 2010, **132**, 7856-7857.
25 C. R. Wade and M. Dinča, *Dalton Trans.*, 2012, **41**, 7931-7938.
26 Z. Hulvey, B. Vlaisavlijevich, J. A. Mason, E. Tsivion, T. P. Dougherty, E. D. Bloch, M. Head-Gordon, B. Smit, J. R. Long and C. M. Brown, *J. Am. Chem. Soc.*, 2015, **137**, 10816-10825.
27 F. A. Cotton, L. M. Daniels, C. Lin and C. A. Murillo, *Chem. Commun.*, 1999, 841-842.
28 F. A. Cotton, C. Lin and C. A. Murillo, *Inorg. Chem.*, 2001, **40**, 6413-6417.
29 G. R. Lorzing, E. J. Gosselin, B. S. Lindner, R. Bhattacharjee, G. P. A. Yap, S. Caratzoulas and E. D. Bloch, *Chem. Commun.*, 2019, **55**, 9527-9530.
30 C. G. Espino, K. W. Fiori, M. Kim and J. Du Bois, *J. Am. Chem. Soc.*, 2004, **126**, 15378-15379.
31 R. J. Pakula, A. M. Martinez, E. A. Noten, C. F. Harris and J. F. Berry, *Polyhedron*, 2019, **161**, 93-103.
32 J. B. Diccianni, C. Hu and T. Diao, *Angew. Chem. Int. Ed.*, 2017, **56**, 3635-3639.
33 D. C. Powers and T. Ritter, *Nat. Chem.*, 2009, **1**, 302-309.
34 J. E. Barker and T. Ren, *Inorg. Chem.*, 2008, **47**, 2264-2266.
35 Y. L. Tnay, C. Chen, Y. Y. Chua, L. Zhang and S. Chiba, *Org. Lett.*, 2012, **14**, 3550-3553.
36 J.-H. Deng, J. Luo, Y.-L. Mao, S. Lai, Y.-N. Gong, D.-C. Zhong and T.-B. Lu, *Sci. Adv.*, 2020, **6**, eaax9976.
37 G. Men and J.-M. Lehn, *J. Am. Chem. Soc.*, 2017, **139**, 2474-2483.
38 M. M. Deegan, A. M. Antonio, G. A. Taggart and E. D. Bloch, *Coord. Chem. Rev.*, 2021, **430**, 213679.
39 C. D. Charles and E. D. Bloch, *Supramolecular Chemistry*, 2019, **31**, 508-513.
40 B. M. Connolly, D. G. Madden, A. E. H. Wheatley and D. Fairen-Jimenez, *J. Am. Chem. Soc.*, 2020, **142**, 8541-8549.
41 A. Carné-Sánchez, G. A. Craig, P. Larpent, T. Hirose, M. Higuchi, S. Kitagawa, K. Matsuda, K. Urayama and S. Furukawa, *Nat. Commun.*, 2018, **9**, 2506.
42 M. L. Schneider, O. M. Linder-Patton and W. M. Bloch, *Chem. Commun.*, 2020, **56**, 12969-12972.
43 D. Nam, J. Huh, J. Lee, J. H. Kwak, H. Y. Jeong, K. Choi and W.

Choe, *Chem. Sci*., 2017, **8**, 7765-7771.